# Supporting Information

## Swietach et al. 10.1073/pnas.1222433110

### Mathematical Supplement

**Parameters.** Parameters are presented in Table S1.

**Model Equations.** The model was solved over a 1D domain (120 μm), assuming uniform concentration in the radial dimension. A pH gradient was imposed by enforcing a fixed boundary condition for $[H^+] = 10^{-6.6}$ M on the proximal end of the myocytes and $[H^+] = 10^{-7.2}$ M on the opposite end of the myocytes. Initial intracellular free $[Ca^{2+}]$ and free $[Mg^{2+}]$ were set to 100 nM and 0.75 mM, respectively. Boundary conditions for all solutes, barring free $H^+$ ions, were set to zero flux (i.e., reflection). The model consisted of a system of 23 parabolic differential equations, each representing 1 of the 23 participating solutes ($U = [u_1,\ldots u_{23}]$; see Table S1), and it was solved using the pdepe function of MATLAB (MathWorks):

$$\partial U/\partial t = D \times \partial^2 U/\partial t^2 + f(U).$$

Vector D defines the diffusion coefficients of participating solutes. Function $f$ defines the kinetics of binding between a buffer (Buf) and ligand ($X = H^+$, $Ca^{2+}$, or $Mg^{2+}$), given as:

$$\partial[BufX]/\partial t = q^x \times [X] \times [Buf] - q^x \times K^x_{Buf} \times [BufX].$$

$[H^+]$ sensitivity of $Ca^{2+}$ binding to fast $Ca^{2+}$ buffers (pooling troponin C, calmodulin, and sarcoplasmic reticulum $Ca^{2+}$ pump) was coded by scaling the $Ca^{2+}$-binding rate constant by a factor of $H^+/(H^+ + K^H_{fast})$, where $K^H_{fast}$ is the acid dissociation constant. The value of $K^H_{fast}$ was set $10^{-6.5}$ M, which allows for a sufficient release of $Ca^{2+}$ during uniform acid loading of the cell. This value simulates the apparent pH sensitivity of $Ca^{2+}$ binding to troponin C (1).

**Inadequacy of Fluo3 to Generate Spatial $Ca^{2+}/H^+$ Interactions.** The exogenous fluorescent dye Fluo3 is, effectively, a mobile $Ca^{2+}/H^+$ buffer because of its affinity for $Ca^{2+}$, and pH sensitivity of fluorescence (2). The dye's apparent acid dissociation constant $pK_H$ was estimated to be ~5.7 based on the $F/F_0$ fall recorded with 1,2-bis(o-aminophenoxy)ethane-N,N,N′,N-tetraacetic acid–pretreated cells exposed to acetate [intracellular pH ($pH_i$) drop from 7.2 to 6.6; Fig. 1 *B*, *v*)]. Under these $Ca^{2+}$-clamp conditions, changes in fluorescence would be due to a pH artifact of the dye. Using the dye's diffusion coefficient in myoplasm [25 $\mu m^2/s$ (3)], the spatial $Ca^{2+}/H^+$ interaction was simulated assuming no histidyl dipeptide (HDP) or ATP. A $pH_i$ gradient of 0.6 unit produced a longitudinal $[Ca^{2+}]$ gradient of <10 nM with 25 μM Fluo3. Even after raising intracellular Fluo3 concentration by a factor of 1,000, the $[Ca^{2+}]$ gradient was no greater than 15 nM. Thus, Fluo3 alone cannot produce the experimentally observed spatial $Ca^{2+}/H^+$ interaction.

**Inadequacy of Plasmalemmal $Ca^{2+}/H^+$ Pump to Generate Spatial $Ca^{2+}/H^+$ Interactions.** The plasmalemmal $Ca^{2+}$ ATPase (PMCA) has been proposed to function as a $Ca^{2+}/H^+$ exchanger (4). Hypothetically, it is possible for PMCA-mediated $Ca^{2+}/H^+$ exchange to produce a local rise in $[Ca^{2+}]$ in the acidic microdomain. If the $[H^+]$ microdomain were maintained, the $[Ca^{2+}]$ gradient established by regional PMCA activity would also be stable. To test whether PMCA could provide a mechanistic explanation for the experimentally observed spatial $Ca^{2+}/H^+$ interactions, the model was modified to introduce a boundary flux term for free $Ca^{2+}$ ions. PMCA flux ($J_p$) was defined by a Hill equation (5, 6):

$$J_p = V_{max} \times [Ca^{2+}]^n / \left([Ca^{2+}]^n + K_p^n\right).$$

The pump's maximal transport rate ($V_{max}$), Hill cooperativity (n), and $Ca^{2+}$ affinity ($K_p$) at pH = 7.2 were set to 2.2 μM/s, 1.6, and 0.5 μM, respectively (7). A "leak" $Ca^{2+}$ influx was included in the $Ca^{2+}$ boundary condition to balance $J_p$ at diastolic $[Ca^{2+}]_i$, thus ensuring stable $[Ca^{2+}]_i$ of 100 nM under resting conditions at pH = 7.2. The effect of pH on plasmalemmal $Ca^{2+}$ stoichiometry (PMCA) was simulated by varying $V_{max}$ or $K_p$ (at constant $Ca^{2+}$ leak). The simulation was run in the absence of HDPs and ATP (while keeping the effective $Ca^{2+}$ diffusion coefficient constant). To produce an 80-nM $[Ca^{2+}]$ gradient over a 0.6-unit $pH_i$ gradient, it was necessary to reduce $V_{max}$ by >20-fold or $K_p$ by greater than sevenfold, while maintaining a relatively high sarcolemmal inward leak of 0.16 μM/s. This exceptionally steep $pH_i$ sensitivity and large $Ca^{2+}$ leak were deemed incompatible with the kinetics of PMCA activity and experimental conditions (absence of extracellular $Ca^{2+}$ would curtain inward leak). Thus, $Ca^{2+}/H^+$ exchange on PMCA was deemed highly unlikely as an underlying mechanism for spatial $Ca^{2+}/H^+$ interactions.


1. Crampin EJ, Smith NP, Langham AE, Clayton RH, Orchard CH (2006) Acidosis in models of cardiac ventricular myocytes. *Philos Transact A Math Phys Eng Sci* 364(1842):1171–1186.
2. Minta A, Kao JP, Tsien RY (1989) Fluorescent indicators for cytosolic calcium based on rhodamine and fluorescein chromophores. *J Biol Chem* 264(14):8171–8178.
3. Cordeiro JM, et al. (2001) Location of the initiation site of calcium transients and sparks in rabbit heart Purkinje cells. *J Physiol* 531(Pt 2):301–314.
4. Kuwayama H (1988) The membrane potential modulates the ATP-dependent $Ca^{2+}$ pump of cardiac sarcolemma. *Biochim Biophys Acta* 940(2):295–299.
5. Choi HS, Eisner DA (1999) The role of sarcolemmal $Ca^{2+}$-ATPase in the regulation of resting calcium concentration in rat ventricular myocytes. *J Physiol* 515(Pt 1): 109–118.
6. Bassani JW, Bassani RA, Bers DM (1994) Relaxation in rabbit and rat cardiac cells: species-dependent differences in cellular mechanisms. *J Physiol* 476(2):279–293.
7. Shannon TR, Wang F, Puglisi J, Weber C, Bers DM (2004) A mathematical treatment of integrated Ca dynamics within the ventricular myocyte. *Biophys J* 87(5): 3351–3371.

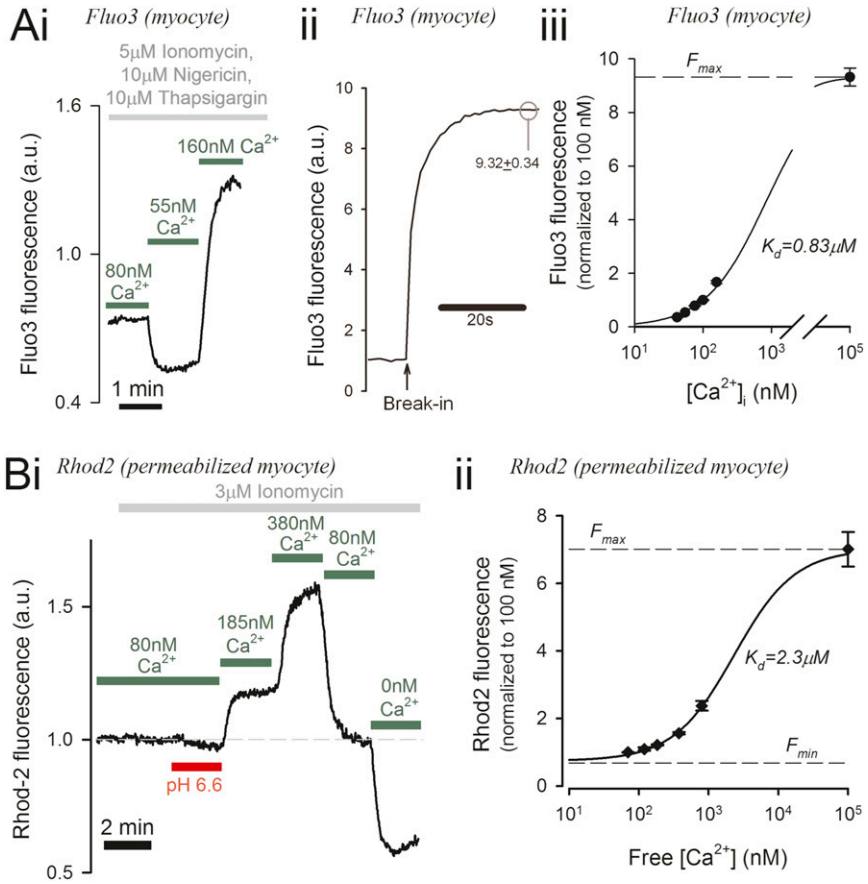


**Fig. S1.** Calibration of $Ca^{2+}$ indicator dyes in cardiac ventricular myocytes. (*A*) Calibration of Fluo3. (*i*) Fluo3 acetoxymethyl (AM)-loaded myocyte, superfused in high-$K^+$ buffer [140 mM KCl, 20 mM Hepes, 0.5 mM EGTA, 1 mM $MgCl_2$ (pH 7.2)] containing 10 μM thapsigargin [to block sarcoplasmic reticulum $Ca^{2+}$ (SERCA)], 10 μM nigericin (to equilibrate intra- and extracellular pH), and 5 μM ionomycin (to equilibrate intra- and extracellular $Ca^{2+}$). Extracellular $Ca^{2+}$ was varied by adding $CaCl_2$ to attain $[Ca^{2+}]_i$ as indicated (calculated using CaBuf software; G. Droogmans, Leuven, Belgium). (*ii*) Fluo3 AM-loaded myocyte superfused in 0Na-0Ca solution containing 10 mM 2,3-butanedione monoxime (to block contraction) and 10 μM thapsigargin. A patch pipette containing 100 mM K-gluconate, 30 mM KCl, 10 mM Hepes, and 1 mM $CaCl_2$ at pH 7.2 was attached to cell. Maximal fluorescence at saturating $[Ca^{2+}]$ was measured after perforating the membrane under the patch pipette with suction. (*iii*) Calibration curve. (*B*) Calibration of Rhod2 in saponin-permeabilized cells treated with 3 μM ionomycin. (*i*) Extramitochondrial $[Ca^{2+}]$ was varied by changing the total $[Ca^{2+}]$ added to 1,2-bis(o-aminophenoxy)ethane-N,N,N′,N′-tetraacetic acid (BAPTA)-buffered solutions (calculated using CaBuf software). (*ii*) Calibration curve.

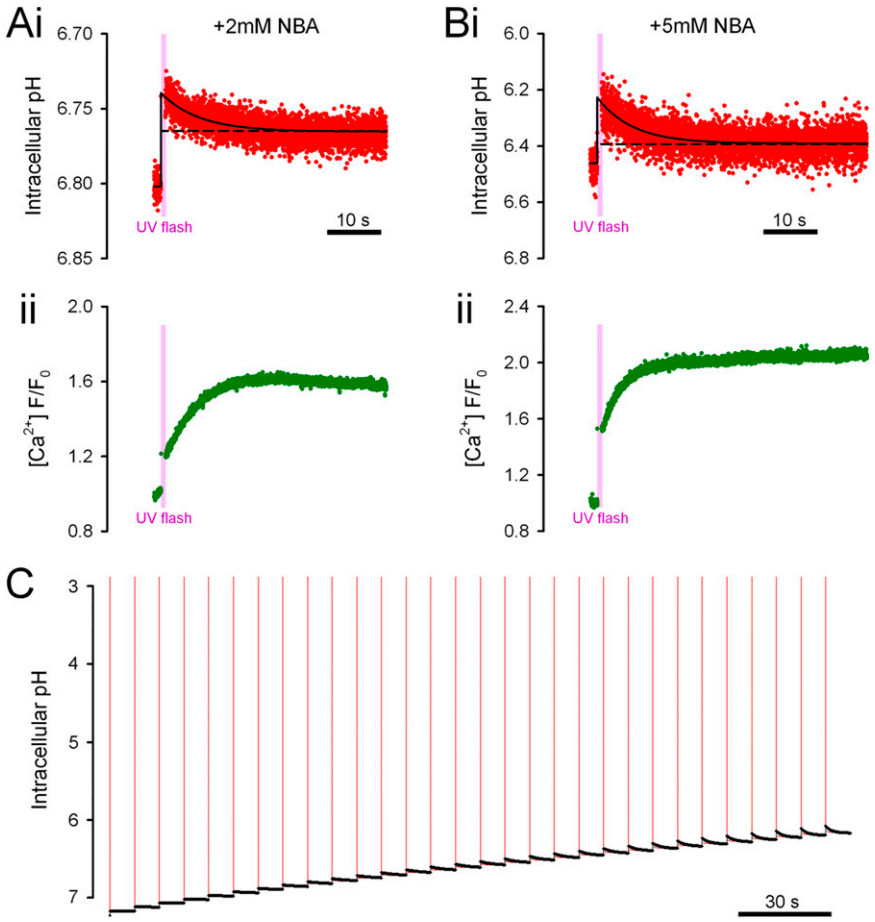


**Fig. S2.** Photolytic uncaging of $H^+$ ions drives intrinsic buffers out of equilibrium. (*A*) Single, whole-cell UV flash applied to cell superfused with 0Na-0Ca solution containing 2 mM 2-nitrobenzaldehyde (NBA), the membrane-permeant caged $H^+$ compound. (*i*) Fast time-base recordings show that pH (measured in cSNARF1 [5-(and-6)-carboxyseminaphtharhodafluor-1]-loaded myocytes) relaxes to its equilibrium level with a time constant of ~6 s. The dashed line shows equilibrium pH, predicted from buffering capacity measurements (1). (*ii*) Photolytic $H^+$ release evokes a delayed rise in $[Ca^{2+}]$ (measured in Fluo3-loaded myocytes; $n = 5$). (*B*) Experiments in *A* repeated with 5 mM NBA ($n = 5$). (*C*) Three-buffer mathematical model of $pH_i$ dynamics [featuring two intrinsic buffers (2) and the pH-sensitive dye cSNARF1] was used to simulate the actual (red) and cSNARF1-reported (black) $pH_i$ time course during repeated (once every 9 s) uncaging from 1 mM NBA. The cSNARF1-reported $pH_i$ time course was derived using the Henderson–Hasselbalch equation from the concentration of protonated and unprotonated dye. The concentration and pK (measure of apparent $H^+$ affinity) of cSNARF1 were 400 μM and 7.5, respectively (3). The relatively slow kinetics of buffering allow for large $pH_i$ excursions during rapid photolytic $H^+$ uncaging.

1. Zaniboni M, et al. (2003) Intracellular proton mobility and buffering power in cardiac ventricular myocytes from rat, rabbit, and guinea pig. *Am J Physiol Heart Circ Physiol* 285(3): H1236–H1246.
2. Swietach P, Vaughan-Jones RD (2005) Relationship between intracellular pH and proton mobility in rat and guinea-pig ventricular myocytes. *J Physiol* 566(Pt 3):793–806.
3. Vaughan-Jones RD, Peercy BE, Keener JP, Spitzer KW (2002) Intrinsic H(+) ion mobility in the rabbit ventricular myocyte. *J Physiol* 541(Pt 1):139–158.

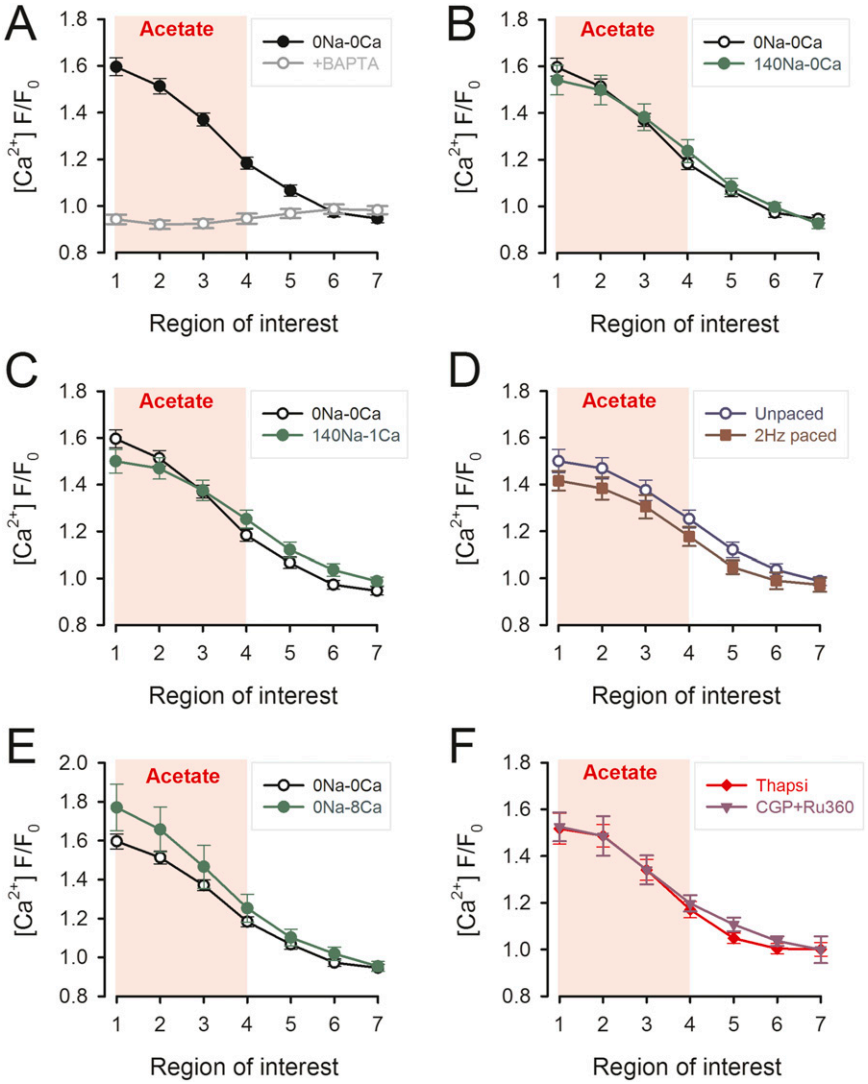


**Fig. S3.** $[Ca^{2+}]$ gradients measured under different experimental conditions in response to a $pH_i$ microdomain. A 0.6-unit longitudinal $pH_i$ gradient was established and maintained by regional exposure of a myocyte to 80 mM acetate using a dual-microperfusion apparatus (with the microstream boundary placed perpendicular to the cell along its center). $[Ca^{2+}]_i$ was imaged in Fluo3-loaded myocytes at 5 min of dual microperfusion. (*A*) In the absence of $Na^+$ (replaced with NMDG) and $Ca^{2+}$ (replaced with EGTA), regional exposure to acetate in 0Na and 0Ca microstreams produced a large $[Ca^{2+}]_i$ gradient ($n = 25$), which was abolished in cells preloaded with the $Ca^{2+}$ buffer BAPTA (100 μM, AM-loaded; $n = 18$). (*B*) Raising $[Na^+]$ in both microstreams to the physiological level of 140 mM did not affect the $[Ca^{2+}]_i$ gradient ($n = 15$). Cariporide (30 μM) was added to both microstreams to inhibit sarcolemmal $Na^+/H^+$ exchange (NHE). (*C*) Raising $[Na^+]$ and $[Ca^{2+}]$ in both microstreams to their physiological levels of 140 mM and 1 mM, respectively, did not affect the $[Ca^{2+}]_i$ gradient ($n = 9$). Cariporide (30 μM) was added to both microstreams to inhibit NHE. To account for $Ca^{2+}$ binding to acetate, total $[Ca^{2+}]$ in the acetate-containing microstream was 1.2 mM (giving 1 mM $[Ca^{2+}]_i$, confirmed with a $Ca^{2+}$ microelectrode). (*D*) Experiment in normal extracellular $Na^+$ and $Ca^{2+}$ repeated on electrically paced myocytes (2-Hz field stimulation), showing no effect of excitation/contraction coupling on the $pH_i$-evoked $Ca^{2+}$ gradient ($n = 18$). (*E*) $[Ca^{2+}]_i$ gradients were only modestly increased when $Ca^{2+}$ extrusion on PMCA was blocked by raising extracellular $Ca^{2+}$ to 8 mM, following a 3-min cell pretreatment in 0Na-0Ca solution ($n = 7$). (*F*) Experiments in the absence of extracellular $Na^+$ and $Ca^{2+}$ performed on myocytes treated with thapsigargin (Thapsi) to inhibit SERCA activity and empty the sarcoplasmic reticulum (SR; 10-min pretreatment with 10 μM Thapsi; $n = 20$) or on myocytes exposed to the mitochondrial $Na^+/Ca^{2+}$ blocker CGP-37157 (20 μM) and the $Ca^{2+}$-uniporter blocker ruthenium-360 (Ru360; 5 μM) to block $Ca^{2+}$ fluxes in and out of mitochondria ($n = 7$). Neither treatment abolished the $[Ca^{2+}]_i$ gradients.

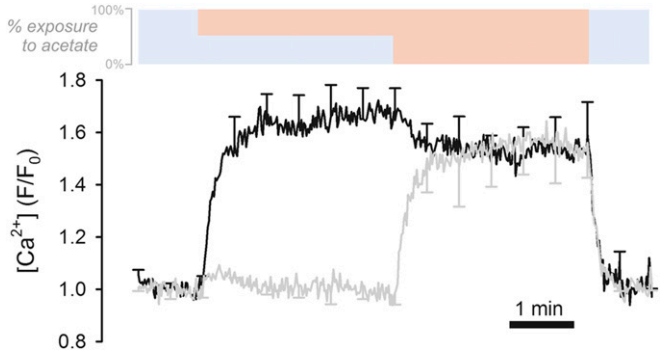


**Fig. S4.** Local exposure to 80 mM acetate (shaded in pink) produces a $[Ca^{2+}]_i$ gradient that does not dissipate, reaching $[Ca^{2+}]_i$ at the proximal (acetate-exposed) end of 1.67 normalized fluorescence ($F/F_0$) units. On subsequent whole-cell exposure to acetate, distal $[Ca^{2+}]_i$ rises to 1.56 $F/F_0$, whereas proximal $[Ca^{2+}]_i$ falls by 20% (NB: $[H^+]$ in the proximal region of interest falls by only 10%; Fig. 4 *B*, *i*). During local acetate exposure, proximal $[Ca^{2+}]_i$ is elevated by an active mechanism.

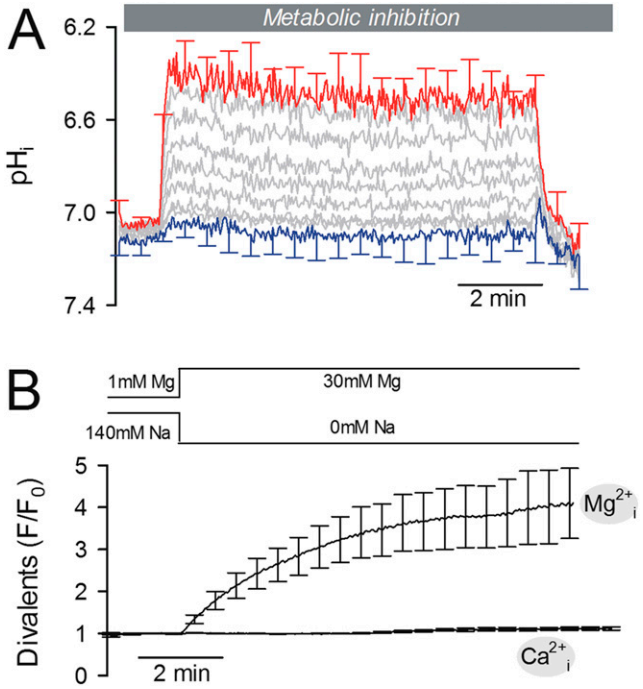


**Fig. S5.** (*A*) $pH_i$ gradient in metabolically inhibited myocytes. A cardiac myocyte was treated with 10 μM rotenone, 10 μM antimycin A, and 5 mM deoxyglucose (in the absence of glucose) to inhibit metabolism. The $pH_i$ gradient was subsequently established by exposing half of the myocyte to 0Na-0Ca solution containing 80 mM acetate and to acetate-free 0Na-0Ca in the remainder of the cell, using dual microperfusion. The $pH_i$ gradient was no different from that produced in control cells without metabolic inhibitors ($n = 15$). (*B*) Loading myocytes with $Mg^{2+}$ using the method of Almulla et al. (1). Myocytes were AM-loaded with either Fluo3, to report cytoplasmic $[Ca^{2+}]$, or MagFluo4, to report cytoplasmic $[Mg^{2+}]$. $Mg^{2+}$ loading was triggered by raising extracellular $Mg^{2+}$ (from 1 to 30 mM) and removing extracellular $Na^+$ (replacing with *N*-methyl-D-glucamine) ($n = 10$ each).

1. Almulla HA, Bush PG, Steele MG, Ellis D, Flatman PW (2006) Loading rat heart myocytes with $Mg^{2+}$ using low-$[Na^+]$ solutions. *J Physiol* 575(Pt 2):443–454.

**Table S1. Parameterization of constants for diffusion-reaction model**

| Parameter | Definition | Value | Reference |
|---|---|---|---|
| $D_H$ | Cytoplasmic free $H^+$ diffusion coefficient | 6000 $\mu m^2/s$ | (1) |
| $D_{Ca}$ | Cytoplasmic free $Ca^{2+}$ diffusion coefficient | 300 $\mu m^2/s$ | (2-4) |
| $D_{Mg}$ | Cytoplasmic free $Mg^{2+}$ diffusion coefficient | 300 $\mu m^2/s$ | as $D_{Ca}$ |
| $q^H$ | $H^+$ binding rate constant | 100 $\mu M^{-1}$ $s^{-1}$ | (1) |
| $q^{Ca}_{fast}$ | $Ca^{2+}$ binding rate constant to fast $Ca^{2+}$ buffer, ATP, HDP, Fluo3. | 30 $\mu M^{-1}$ $s^{-1}$ | (5) |
| $q^{Ca}_{slow}$ | $Ca^{2+}$ binding rate constant to slow $Ca^{2+}$ buffer | 2.4 $\mu M^{-1}$ $s^{-1}$ | (5) |
| $q^{Mg}_{fast}$ | $Mg^{2+}$ binding rate constant to ATP, HDP | 30 $\mu M^{-1}$ $s^{-1}$ | as $q^{Ca}_{fast}$ |
| $q^{Mg}_{slow}$ | $Mg^{2+}$ binding rate constant to slow $Ca^{2+}$ buffer | 0.003 $\mu M^{-1}$ $s^{-1}$ | (5) |
| $C_{fix}$ | Fixed $H^+$-buffer concentration | 62.4 mM | *, (6, 7) |
| $K^H_{fix}$ | Fixed $H^+$-buffer $H^+$ affinity | $10^{-6.30}$ M | *, (6, 7) |
| $D_{mob}$ | Nondipeptide mobile buffer diffusion coefficient | 22 $\mu m^2/s$ | *, (6, 7) |
| $C_{mob}$ | Nondipeptide mobile $H^+$-buffer concentration | 5.67 mM | *, (6, 7) |
| $K^H_{mob}$ | Nondipeptide mobile $H^+$-buffer $H^+$ affinity | $10^{-8.47}$ M | *, (6, 7) |
| $D_{buf}$ | Pooled fast/slow $Ca^{2+}$ buffer diffusion coefficient | 0 $\mu m^2/s$ | |
| $C_{fast}$ | Fast $Ca^{2+}$ buffer concentration | 120 $\mu M$ | (5) |
| $K^{Ca}_{fast}$ | Fast $Ca^{2+}$ buffer $Ca^{2+}$ affinity | $10^{-6.23}$ M | (5) |
| $C_{slow}$ | Slow $Ca^{2+}$ buffer concentration | 140 $\mu M$ | (5) |
| $K^{Ca}_{slow}$ | Slow $Ca^{2+}$ buffer $Ca^{2+}$ affinity | $10^{-7.87}$ M | (5) |
| $K^{Mg}_{slow}$ | Slow $Ca^{2+}$ buffer $Mg^{2+}$ affinity | $10^{-2.95}$ M | (5) |
| $C_{carn}$ | Histidyl-dipeptide concentration | 17 mM | *, (6, 7) |
| $K^H_{carn}$ | Histidyl-dipeptide $H^+$ affinity | $10^{-6.8}$ M | (8) |
| $K^{Ca}_{carn}$ | Histidyl-dipeptide $Ca^{2+}$ affinity | $10^{-3.22}$ M | (8) |
| $K^{Mg}_{carn}$ | Histidyl-dipeptide $Mg^{2+}$ affinity | $10^{-3.1}$ M | (8) |
| $D_{carn}$ | Histidyl-dipeptide diffusion coefficient | 225 $\mu m^2/s$ | *, (6, 7) |
| $C_{atp}$ | ATP concentration | 7.5 mM | (9, 10) |
| $K^H_{atp}$ | ATP $H^+$ affinity | $10^{-6.49}$ M | (11) |
| $K^{Ca}_{atp}$ | ATP $Ca^{2+}$ affinity | $10^{-4.66}$ M | (9) |
| $K^{Mg}_{atp}$ | ATP $Mg^{2+}$ affinity | $10^{-4.36}$ M | (9) |
| $D_{atp}$ | ATP diffusion coefficient | 150 $\mu m^2/s$ | (2) |
| $C_{fluo}$ | Fluo3 concentration | 25 $\mu M$ | (5) |
| $K^H_{fluo}$ | Fluo3 $H^+$ affinity | $10^{-5.7}$ M | Fig. 1B |
| $K^{Ca}_{fluo}$ | Fluo3 $Ca^{2+}$ affinity | $10^{-6.08}$ M | Fig. S1A |
| $D_{fluo}$ | Fluo3 diffusion coefficient | 25 $\mu m^2/s$ | (2) |

Where applicable, parameters corrected to 37°C (2).

*Derived from three-component buffer best-fit to intrinsic $H^+$-mobility and buffering capacity data.


1. Swietach P, Leem CH, Spitzer KW, Vaughan-Jones RD (2005) Experimental generation and computational modeling of intracellular pH gradients in cardiac myocytes. *Biophys J* 88(4): 3018–3037.
2. Cordeiro JM, et al. (2001) Location of the initiation site of calcium transients and sparks in rabbit heart Purkinje cells. *J Physiol* 531(Pt 2):301–314.
3. Kushmerick MJ, Podolsky RJ (1969) Ionic mobility in muscle cells. *Science* 166(3910):1297–1298.
4. Swietach P, Spitzer KW, Vaughan-Jones RD (2008) $Ca^{2+}$-mobility in the sarcoplasmic reticulum of ventricular myocytes is low. *Biophys J* 95(3):1412–1427.
5. Shannon TR, Wang F, Puglisi J, Weber C, Bers DM (2004) A mathematical treatment of integrated Ca dynamics within the ventricular myocyte. *Biophys J* 87(5):3351–3371.
6. Swietach P, Vaughan-Jones RD (2005) Relationship between intracellular pH and proton mobility in rat and guinea-pig ventricular myocytes. *J Physiol* 566(Pt 3):793–806.
7. Swietach P, Spitzer KW, Vaughan-Jones RD (2007) pH-Dependence of extrinsic and intrinsic H(+)-ion mobility in the rat ventricular myocyte, investigated using flash photolysis of a caged-H(+) compound. *Biophys J* 92(2):641–653.
8. Baran EJ (2000) Metal complexes of carnosine. *Biochemistry (Mosc)* 65(7):789–797.
9. Kargacin ME, Kargacin GJ (1997) Predicted changes in concentrations of free and bound ATP and ADP during intracellular Ca2+ signaling. *Am J Physiol Cell Physiol* 273:C1416–C1426.
10. Vaughan-Jones RD, Peercy BE, Keener JP, Spitzer KW (2002) Intrinsic H(+) ion mobility in the rabbit ventricular myocyte. *J Physiol* 541(Pt 1):139–158.
11. Kushmerick MJ (1997) Multiple equilibria of cations with metabolites in muscle bioenergetics. *Am J Physiol* 272(5 Pt 1):C1739–C1747.